

# MeshPad: Interactive Sketch Conditioned Artistic-designed Mesh Generation and Editing

HAOXUAN LI, Technical University of Munich, Germany  
 ZIYA ERKOC, Technical University of Munich, Germany  
 LEI LI, Technical University of Munich, Germany  
 DANIELE SIRIGATTI, AUDI AG, Germany  
 VLADISLAV ROISOV, AUDI AG, Germany  
 ANGELA DAI, Technical University of Munich, Germany  
 MATTHIAS NIESSNER, Technical University of Munich, Germany

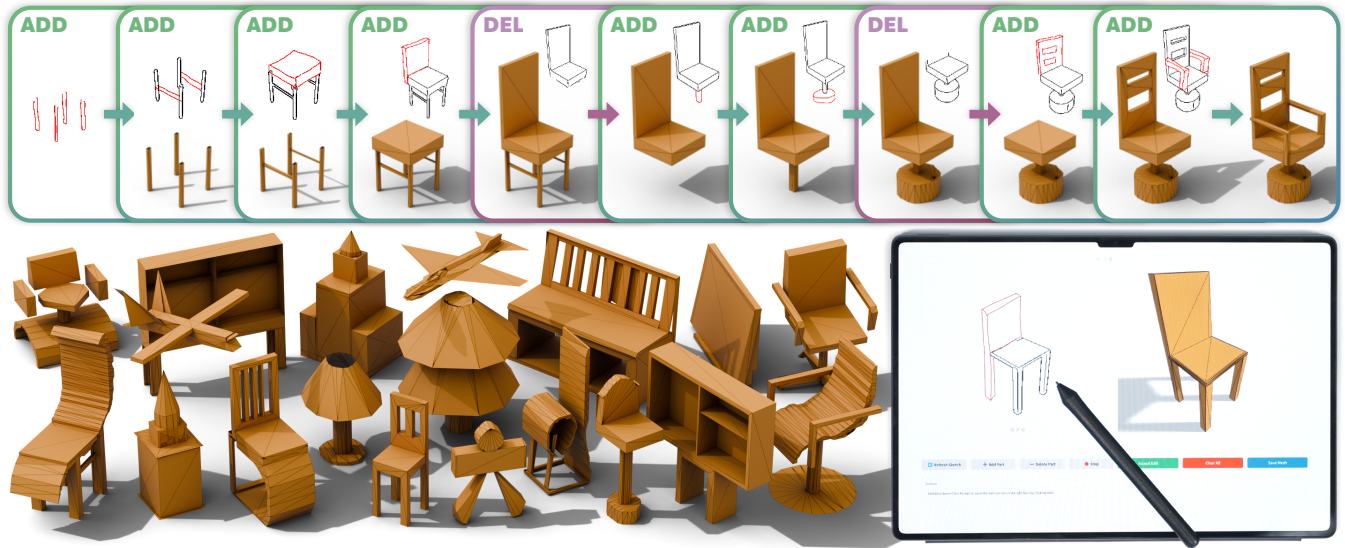


Fig. 1. MeshPad enables interactive mesh creation and editing with sketches. We decompose this complex task into two sketch-conditioned operations: addition and deletion. **Top**: our method allows for a user to create and modify artistic-designed triangle meshes by simply drawing and editing 2D sketches, achieving intuitive and interactive 3D modeling. **Bottom (left)**: our method generates a variety of complex yet compact meshes. **Bottom (right)**: our interactive user interface allows users to iteratively edit the mesh, with each edit step taking a few seconds.

We introduce MeshPad, a generative approach that creates 3D meshes from sketch inputs. Building on recent advances in artistic-designed triangle mesh generation, our approach addresses the need for interactive artistic mesh creation. To this end, we focus on enabling consistent edits by decomposing editing into ‘deletion’ of regions of a mesh, followed by ‘addition’ of new mesh geometry. Both operations are invoked by simple user edits of a sketch image, facilitating an iterative content creation process and enabling the construction of complex 3D meshes. Our approach is based on a triangle sequence-based mesh representation, exploiting a large Transformer model for mesh triangle addition and deletion. In order to perform edits interactively, we introduce a vertex-aligned speculative prediction strategy on top of our additive mesh generator. This speculator predicts multiple output tokens corresponding to a vertex, thus significantly reducing the computational cost of inference and accelerating the editing process, making it

possible to execute each editing step in only a few seconds. Comprehensive experiments demonstrate that MeshPad outperforms state-of-the-art sketch-conditioned mesh generation methods, achieving more than 22% mesh quality improvement in Chamfer distance, and being preferred by 90% of participants in perceptual evaluations.

## 1 INTRODUCTION

Triangle meshes are one of the most predominant 3D representations used in 3D production applications, from video games to virtual reality and movies. Mesh creation and editing is thus a central element of computer graphics. In contrast to 3D representations such as voxels [Dai et al. 2020, 2017; Ren et al. 2024], points [Vahdat et al. 2022; Yang et al. 2019; Zhou et al. 2021], or neural implicit representations [Hertz et al. 2022; Kerbl et al. 2023; Mildenhall et al. 2021], triangle meshes represent surfaces in a compact, structured fashion, as well as enabling efficient fine-scale detail and naturally integrating into modern rendering and editing pipelines, achieving high fidelity with relatively few primitives.

Authors’ addresses: Haoxuan Li, Ziya Erkoc, Angela Dai, Matthias Nießner, and Lei Li (Technical University of Munich, Boltzmannstraße 3, 85748 Garching bei München, Bayern, Germany; {haoxuan.li, ziya.erkoc, angela.dai, niessner}@tum.de, lilei.cg@gmail.com); Daniele Sirigatti and Vladislav Rosov (Audi AG, Munich, Bayern, Germany; {daniele.sirigatti, vladislav.rosov}@audi.de).

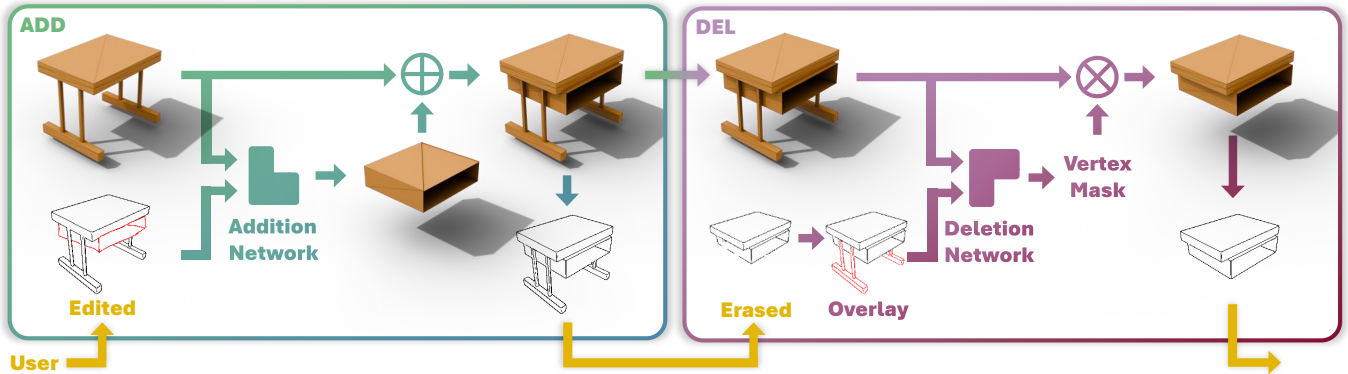


Fig. 2. Method Overview. We show the decomposition of mesh creation and editing into *addition* and *deletion* operations (left and right, respectively). **ADD**: in mesh addition, a transformer generates new mesh regions corresponding to newly added strokes (in red) in the input sketch. The generated mesh triangles are then merged with the existing mesh. **DEL**: in mesh deletion, we show a deletion operation applied to the mesh addition output. We erase sketch strokes to remove corresponding mesh regions, and overlay the erased strokes in red alongside untouched regions to provide more context to the deletion network. We then predict which mesh vertices correspond to regions to be deleted, and prune the mesh accordingly. After each addition or deletion operation, we automatically generate an updated sketch corresponding to the current output mesh, to enable further sketch-based editing.

Recent advances in generative 3D models have shown significant potential in generating 3D meshes directly [Chen et al. 2024b,e; Hao et al. 2024; Siddiqui et al. 2023; Tang et al. 2024]; however, these output meshes are not editable, which is a crucial component for artistic design in content creation. More specifically, artistic content creation is an iterative process that encompasses not only the initial generation, but also requires multiple cycles of manipulation and editing in order to refine an output to achieve a precise artistic vision. In order for such editing to fit with content creation pipelines, various edits must be performed interactively, affecting only the intended region of the mesh.

We thus propose MeshPad, an interactive sketch-based approach for 3D mesh generation and editing. From an input sketch of a shape drawn by a user, we produce a corresponding 3D mesh. The resulting mesh can then be edited simply by editing the sketch. To achieve efficient and precise mesh editing, we decompose this into simpler subtasks: *deletion* and *addition* of mesh geometry by removing or adding strokes in the sketch. Crucially, this modeling paradigm also leads to easy supervised training of both deletion and addition of elements in the mesh (by simply removing and adding back parts of ground-truth meshes), without requiring collection of real mesh editing sequences for supervision. Our editing-based approach allows for the generation of more complex triangle meshes by iteratively applying a series of edits to construct the final shape.

Algorithmically, MeshPad leverages a hybrid approach combining an autoregressive network for addition and a token-classification network for deletion. Unlike existing artistic-designed mesh generation methods, our addition network generates partial shapes only corresponding to new sketch strokes, rather than repeatedly synthesizing the entire mesh. This naturally solves the problem of preserving unedited mesh regions during editing. Additionally, based on the triangle sequence representation [Chen et al. 2024e], we introduce a vertex-aligned speculative decoder to accelerate autoregressive generation and reduce computational time. Instead of predicting one vertex coordinate at a time, the speculator allows us to predict 3 coordinates, i.e., one vertex, at a time. We find

that jointly training the speculative head and aligning it with the vertex tokens reduces generation time while maintaining generation quality. Furthermore, we implemented a user interface that allows users to interactively edit 3D meshes by drawing 2D sketches. Extensive experiments show that our method outperforms state-of-the-art methods in sketch-conditioned mesh generation, producing cleaner meshes that more accurately align with the sketch input and excelling in partial mesh editing tasks. Finally, our speculative prediction acceleration enables interactive mesh generation and editing within seconds while maintaining overall shape quality.

In summary, our contributions are:

- We introduce a novel method for interactive mesh creation and editing by decomposing the process into addition and deletion. This enables easy training without requiring collection of edited ground-truth meshes, and enables finer-grained control over an iterative 3D mesh creation process.
- Our vertex-aligned speculative classification head for addition notably accelerates the triangle mesh generation by 2.2× without quality loss.

## 2 RELATED WORK

**3D Mesh Generation.** Direct mesh generation offers the compelling advantage of producing outputs that closely resemble artist-crafted 3D shapes. Early approaches proposed various parameterizations of an irregular mesh structure, including atlases [Groueix et al. 2018] and graphs [Dai and Nießner 2019]. Recently, Polygen [Nash et al. 2020] and MeshGPT [Siddiqui et al. 2023] have demonstrated the remarkable potential of transformers in autoregressively generating artistic meshes. Follow-ups such as MeshAnything [Chen et al. 2024b], MeshAnything V2 [Chen et al. 2024e], EdgeRunner [Tang et al. 2024], and Meshtron [Hao et al. 2024] each proposed improvements in tokenization, attention mechanisms, or shape coverage, pushing the limit of direct mesh generation. PolyDiff [Alliegro et al. 2023] instead uses a diffusion backbone for polygonal mesh synthesis. Despite solid progress, these methods focus on full-shape generation and cannot easily handle local editing tasks.

**Conditional 3D Generation.** The history of sketch-driven methods starts with techniques that inflate 2D contours [Igarashi et al. 1999; Nealen et al. 2007] or retrieve 3D models from sketch-based queries [Eitz et al. 2012; Funkhouser et al. 2003]. Modern sketch-based 3D generation methods typically rely on either single-shot generation SDF diffusion models [Robin Borth 2024; Zheng et al. 2023] or direct editing of neural fields [Mikaeili et al. 2023], which usually struggle to output tidy, artistically crafted meshes.

With the advancement in large text-to-image models, DreamFusion [Poole et al. 2023] proposes score distillation sampling with 2D diffusion for text-to-3D generation, followed by Magic3D [Lin et al. 2023], Fantasia3D [Chen et al. 2023b], and Meta 3D AssetGen [Siddiqui et al. 2024]. Text conditions lack precision for fine-grained control [Xu et al. 2023] and additional image condition is often required [Bala et al. 2024; Qian et al. 2024]. In contrast, our method uses iterative sketch conditioning for fine-grained shape control.

**3D Shape Editing.** With the same concept of SDS, many 3D shape editing methods rely on neural representations [Khalid et al. 2025; Liu et al. 2025], and use region-specific masks [Barda et al. 2024; Chen et al. 2024d,a]. SPAGHETTI [Hertz et al. 2022], SALAD [Koo et al. 2023], and PartGen [Chen et al. 2024c] advance part-level neural shape editing by enabling disentangled control, diffusion-based manipulation, and multi-view diffusion for generating and editing meaningful 3D parts, respectively.

Recently, sketch-based 3D editing has emerged as an intuitive alternative to text- and image-based methods. SKED [Mikaeili et al. 2023] and SketchDream [Liu et al. 2024] leverage sketch-conditioned 2D diffusion models for 3D modeling. Other approaches, including SENS [Binniger et al. 2024], Doodle your 3D [Bandyopadhyay et al. 2024], and Masked LRM [Gao et al. 2024], focus on abstraction-aware part manipulation, robust part isolation, and masked reconstruction for fast local edits, respectively.

However, such works struggle to produce an artistic mesh. Techniques based on polygonal meshes or other explicit representations can rely on an expensive optimization [Aigerman et al. 2022; Gao et al. 2023], deformation priors [Tang et al. 2022], specialized parametric families [Elrefaie et al. 2024] or procedural generators [Zhao et al. 2024]. Such approaches do not generalize easily to arbitrary geometry and have difficulties making local edits without conflicting with the global constraints. By contrast, our approach addresses these issues using a sequence-based mesh representation to perform partial editing by removing and then adding triangles.

**Speculative Decoding.** Finally, to reduce inference time for our autoregressive network, we adopt a concept of “speculative decoding”, analogous to language Transformers that generate multiple tokens in one pass [Chen et al. 2023a; Leviathan et al. 2023; Miao et al. 2023; Wertheimer et al. 2024]. We design a vertex-aligned speculator for the mesh sequence to accelerate partial additions, enabling agile and expressive iterative mesh editing.

### 3 METHOD

MeshPad enables interactive mesh creation and editing by iteratively performing addition and deletion operations guided by input sketches. An input sketch image  $\mathcal{I}$  guides the generation of a 3D mesh  $\mathcal{M}$  as a sequence of mesh triangles.  $\mathcal{M}$  can be further edited

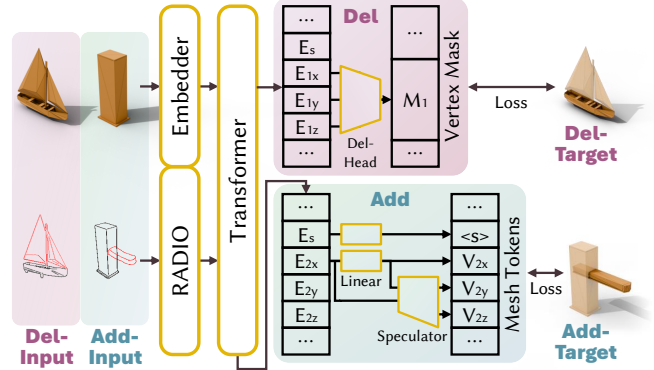


Fig. 3. Model Architecture. We use the Open Pre-trained Transformer (OPT) as the Transformer backbone to process the embedded triangle sequence and the sketch embeddings from a pre-trained image foundation model, RADIO. **Top (right):** the **deletion** network is a classification network that labels each input mesh vertex for removal. The deletion head takes the  $xyz$  coordinate embeddings of a vertex as input and produces a masking label for the vertex. **Bottom (right):** the **addition** network is an autoregressive generation model that predicts new mesh tokens with a speculator. During the speculative prediction, we align the speculator to the vertex axis so that it always takes the  $x$  coordinate as input and predicts the vertex’s  $y$  and  $z$  coordinates. Note that  $E$ ,  $M$ ,  $V$ , and  $\langle s \rangle$  represent Transformer hidden states, vertex masks, vertex coordinate tokens, and the  $\langle \text{split} \rangle$  token, respectively.

by removing strokes from  $\mathcal{I}$  to delete mesh regions, or adding new strokes to introduce new geometry. To achieve interactive rates for editing, we introduce a vertex-aligned speculator into our mesh addition transformer, significantly accelerating its autoregressive generation. An overview of our approach is shown in Fig. 2.

#### 3.1 Mesh Creation and Editing

We decouple sketch-based mesh creation and editing into two sub-tasks: addition and deletion. Both mesh operations are conditioned on a sketch image  $\mathcal{I}$ , a bitmap where colored line strokes indicate regions to be added or deleted. We define a mesh  $\mathcal{M}$  as a sequence of triangles  $\mathcal{M} = \{\mathcal{F}\}$ , where  $\mathcal{F} = \{v_1, v_2, v_3\}$  and  $v \in \mathbb{R}^3$  represents 3D vertex locations.

Line strokes in the input sketch image  $\mathcal{I}$  are divided into two mutually exclusive sets,  $\mathcal{I}_k$  and  $\mathcal{I}_r$ , colored black and red in our visualizations, respectively. When performing an addition or deletion,  $\mathcal{I}_r$  corresponds to the user edit, i.e., the part to be added or deleted, respectively, while  $\mathcal{I}_k$  represents the untouched sketch regions. We denote the mesh parts corresponding to  $\mathcal{I}_r$  and  $\mathcal{I}_k$  as mutually exclusive sets  $\mathcal{M}_r$  and  $\mathcal{M}_k$ , respectively, and thus  $\mathcal{M}_r \cup \mathcal{M}_k = \mathcal{M}$ . The operation—addition or deletion—is determined by whether the  $\mathcal{I}_r$  is added as new strokes (addition), or erased from existing strokes (deletion). This also enables simple supervision of both deletion and addition networks by removing or adding back random regions of mesh geometry of 3D shapes, without requiring ground-truth sequences of mesh edits (see Sec. 3.4 for more detail).

**Sketch-conditioned Mesh Deletion.** Given a current mesh state  $\mathcal{M}$  and a sketch image  $\mathcal{I}$  containing a non-empty set of deletion strokes  $\mathcal{I}_r$ , the goal is to obtain a mesh  $\mathcal{M}_k \subseteq \mathcal{M}$  that excludes parts

corresponding to  $\mathcal{I}_r$ . This is formulated as a binary classification task over the sequence of triangles composing  $\mathcal{M}$ ; those predicted as corresponding to  $\mathcal{I}_r$  are then removed.

We employ a transformer-based architecture (Sec. 3.2) to predict a binary label for each vertex in the mesh sequence, forming a set of vertices  $\mathcal{V}'_r$  corresponding to  $\mathcal{I}_r$ . Then we predict the target mesh  $\mathcal{M}'_k$  by deleting triangles with any vertex predicted as deleted:

$$\mathcal{M}'_r = \{\mathcal{F} \in \mathcal{M} \mid \exists v \in \mathcal{F} : v \in \mathcal{V}'_r\}; \quad \mathcal{M}'_k = \mathcal{M} \setminus \mathcal{M}'_r. \quad (1)$$

We train this by automatically generating 2D sketches and removal regions from 3D shapes in a self-supervised fashion (Sec. 3.4) to obtain the ground truth  $\mathcal{V}_r = \bigcup_{\mathcal{F} \in \mathcal{M}_r} \mathcal{F}$  and set the binary label of each vertex as:

$$l_v = \begin{cases} 0 & \text{if } v \in \mathcal{V}_r, \\ 1 & \text{otherwise.} \end{cases} \quad (2)$$

This deletion is trained with a binary cross-entropy loss between the predicted binary probability per vertex and the vertex label. Once deletion is performed, we assign  $\mathcal{M} \leftarrow \mathcal{M}'_k$  and  $\mathcal{M}_k \leftarrow \mathcal{M}'_k$ , and automatically generate the updated  $\mathcal{I}_k$  corresponding to the new output mesh  $\mathcal{M}$  (Sec. 3.4), which can be further edited.

**Sketch-conditioned Mesh Addition.** The addition task is the inverse process of deletion. The input is a mesh  $\mathcal{M}_k$  and a sketch  $\mathcal{I}$  containing non-empty  $\mathcal{I}_r$ , and the goal is to generate the mesh  $\mathcal{M}$ . We use a similar architecture as with deletion to autoregressively generate tokens of  $\mathcal{M}'_r$  and merge it with  $\mathcal{M}_k$  to obtain the predicted mesh  $\mathcal{M}'$ . This is supervised by a cross-entropy loss between the ground-truth mesh tokens of  $\mathcal{M}_r$  and the predicted token probabilities. After merging, we assign  $\mathcal{M} \leftarrow \mathcal{M}'$  and  $\mathcal{M}_k \leftarrow \mathcal{M}'$ .

We automatically generate an updated sketch  $\mathcal{I}_k$  reflecting the latest mesh geometry. This enables iterative mesh generation and editing. A user first draws a sketch to produce an initial mesh or loads in a mesh from which we automatically generate a corresponding sketch. Editing can then be performed on this initial mesh and sketch; a user can erase a sketch part with an eraser tool, labeling part of  $\mathcal{I}_k$  as  $\mathcal{I}_r$  and triggering deletion of the corresponding mesh part. The user can also draw new strokes alongside the current  $\mathcal{I}_k$  to introduce new mesh geometry. This iterative editing process avoids re-synthesis of the whole shape, preserving mesh structures in unedited regions. Note that mesh generation from scratch is treated as addition to an empty mesh.

### 3.2 Network Architecture

The detailed model structure is shown in Fig. 3. We use a pre-trained image encoder RADIO 2.5-h [Ranzinger et al. 2024] to encode the sketch input as tokens. We follow MeshAnythingV2 [Chen et al. 2024e] to use the same Open Pre-trained Transformer (OPT) [Zhang et al. 2022] network as our backbone. We also adopt the tokenizer  $\mathcal{T}$  from MeshAnythingV2 to transform a mesh into a sequence  $S = \mathcal{T}(\mathcal{M})$ . The sequence  $S$  is defined as an ordered list consisting of control tokens (<split>, <start>, <end>) and vertex coordinate tokens  $V$ . The <start> and <end> tokens indicate the bounds of the sequence. The <split> token splits the sequence into subsequences containing only vertex tokens, which define a series of adjacent triangles [Chen et al. 2024e].

To perform mesh addition, we use the OPT model to autoregressively predict the next sequence token  $S'_r^{(i+1)}$  given the sketch  $\mathcal{I}$ , input mesh sequence  $S_k = \mathcal{T}(\mathcal{M}_k)$ , and the previously generated tokens  $S'_r^{(1...i)}$ :

$$P\left(S'_r^{(i+1)} \mid S_k, \mathcal{I}, S'_r^{(1...i)}\right) = \text{OPT}\left(S_k, \mathcal{I}, S'_r^{(1...i)}\right). \quad (3)$$

After generating the sequence  $S'_r$ , we obtain an output mesh by detokenizing  $S'_r$  and merging it with the input partial mesh:

$$\mathcal{M}' = \mathcal{M}_k \cup \mathcal{T}^{-1}(S'_r). \quad (4)$$

Instead of generating one token at a time, we introduce a vertex-aligned speculator to predict multiple tokens in a single run (Sec. 3.3).

The deletion network predicts a mask label for each vertex with a deletion head, which processes the encoded states of every three coordinate tokens corresponding to a vertex. While using the same OPT architecture, the attention layers are switched to perform bi-directional attention for each position to capture the global context. After the inference, we aggregate  $\mathcal{V}'_r$  according to Eq. 2, and then obtain the deleted mesh with Eq. 1.

### 3.3 Vertex-aligned Speculator

As we perform mesh addition autoregressively, generating an  $n$ -token sequence requires  $n$  forward passes, significantly limiting mesh generation speed for interactive applications. One effective way of accelerating generation is to use a speculator to generate multiple tokens in a single run. In contrast to natural language, a tokenized mesh sequence contains strong low-level structure – each vertex  $v$  is defined by exactly 3 tokens  $V_{\{x,y,z\}}$  representing its  $x$ ,  $y$ , and  $z$  coordinates. Aligning the speculator with vertex tokens by letting it predict only  $V_{\{y,z\}}$ , as shown in Fig. 3, ensures a consistent context of input and output for the speculator.

We adopt the MLP speculator described in [Wertheimer et al. 2024]. In natural language processing tasks, a speculator can be trained with a frozen pre-trained large language model to accelerate generation. However, in our experiments, we found that this results in performance degradation. We thus train our speculator jointly with the mesh addition task, so that the addition transformer learns to inform the speculator with contextual information in hidden states.

As shown in Fig. 3, the speculator predicts the  $y, z$  coordinates of a vertex  $v'$  by:

$$P\left(V'_{\{y,z\}}\right) = \text{Speculator}\left(E_x, V'_x\right), \quad (5)$$

where  $E_x$  represents Transformer hidden states corresponding to  $V_x$ . The speculator is trained with a cross-entropy loss between ground truth  $V_{\{y,z\}}$  and the prediction. When jointly trained with OPT, the OPT loss function supervises  $V_x$  and control tokens only.

### 3.4 Self-Supervised Data Generation for Mesh Editing

By decomposing sketch-conditioned mesh editing into separate deletion and addition subtasks, we can generate training data for each subtask from 3D shape datasets without requiring real mesh editing sequences.

Given a complete 3D mesh sample  $\mathcal{M}_c$ , we select its triangles to form two mutually exclusive subsets  $\mathcal{M}_r$  and  $\mathcal{M}_k$ , representing



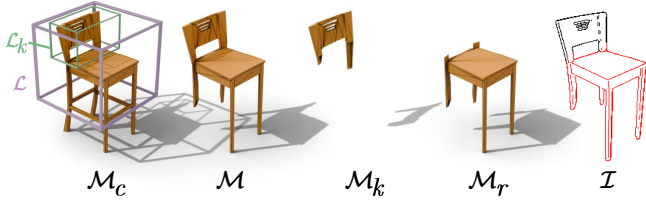


Fig. 4. An example of training data generation: the volume  $\mathcal{L}$  is sampled to cover a large portion from the top, while  $\mathcal{L}_k$  covers the chair backrest. The mesh  $\mathcal{M}$  and  $\mathcal{M}_k$  contains triangles with any vertex in  $\mathcal{L}$  and  $\mathcal{L}_k$ , respectively.  $\mathcal{M}_r$  is the difference between  $\mathcal{M}$  and  $\mathcal{M}_k$ . The red and black line strokes in sketch  $\mathcal{I}$  corresponds to  $\mathcal{M}_k$ , and  $\mathcal{M}_r$ , respectively.

the edited and unedited parts, respectively. Note that  $\mathcal{M}_r \cup \mathcal{M}_k = \mathcal{M}_c$  is not required, as intermediate meshes during editing can be incomplete before deletion or after addition. To achieve this, we sample two volumes  $\mathcal{L}$  and  $\mathcal{L}_k \subseteq \mathcal{L}$  within the bounding volume of  $\mathcal{M}_c$ . An example is shown in Fig. 4. For each volume, we crop a partial mesh by selecting all triangles containing at least one vertex within the given volume:

$$\mathcal{M} = \{\mathcal{F} \in \mathcal{M}_c | \exists \mathbf{p} \in \mathcal{F} : \mathbf{p} \in \mathcal{L}\}, \quad (6)$$

and the same for  $\mathcal{M}_k$ ,  $\mathcal{L}_k$ . We then compute  $\mathcal{M}_r = \mathcal{M} \setminus \mathcal{M}_k$ , which is mutually exclusive from  $\mathcal{M}_k$ . We provide more details about the volume sampling and mesh cropping in the supplementary. The obtained meshes are then used to supervise both the addition and the deletion network in the tasks defined in Sec. 3.1.

**Sketch Generation.** We generate synthetic sketches corresponding to the processed mesh data. During training, this is done automatically through Canny edge detection; at test time, any human-drawn sketch can be used. Fig. 4 shows our data generation process.

Automatic sketch generation is done by applying Canny edge detection on the rendered depth and normal images of  $\mathcal{M}$ . We then merge the two edge detection results to obtain the corresponding synthetic sketch used for training. To get mutually exclusive sets of line strokes  $\mathcal{I}_{\{r,k\}}$ , which correspond to different parts of the mesh, we further render a visibility mask of  $\mathcal{M}_r$  in the same camera view and collect all line strokes within the mask as  $\mathcal{I}_r$ .  $\mathcal{I}_k$  is then defined as the line strokes not in  $\mathcal{I}_r$ . During training, we randomly sample camera views from the upper unit viewing hemisphere, with azimuth angles in  $[-90^\circ, 90^\circ]$  and elevation angles in  $[0^\circ, 60^\circ]$ .

## 4 EXPERIMENTS

### 4.1 Implementation Details

**Data.** Following MeshGPT [Siddiqui et al. 2023] and MeshAnythingV2 [Chen et al. 2024e], we preprocess and filter the ShapeNet dataset [Chang et al. 2015] to obtain approximately 28k meshes from 55 categories, which each have a face count  $< 768$  for training. We sample around 500 meshes for validation and 1000 meshes for testing. Other meshes are used for training.

**Training.** Both the mesh addition and deletion networks are initialized using the OPT weights from the MeshAnythingV2 checkpoint, with the RADIO image model frozen throughout training. We employ a learning rate schedule from  $1 \times 10^{-4}$  to  $1 \times 10^{-6}$ . For the

addition model, training begins with a batch size of 56 for 128 epochs, followed by 20 epochs with a batch size of 224. The deletion model is trained with a batch size of 32 for 128 epochs. Using 4 NVIDIA A100 GPUs, the training process takes approximately 5 days for the addition network and 2 days for the deletion network.

**User Interface.** We develop a Gradio [Abid et al. 2019] user interface to demonstrate our method in an interactive editing environment, accessible from browsers on all types of devices (PC, iPad, etc.). As visualized in Fig. 1, the interface contains a sketchpad for users to draw (addition) and erase (deletion) line strokes and a three.js [Cabello and Contributors 2010] viewer displaying the mesh in real-time. Users can submit their sketches to the addition or deletion job and can always re-sketch and re-submit the job when the outcome should be iterated on. When an edit is accepted, the interface refreshes the sketch in the sketchpad to match the current mesh for further edit, which corresponds to the process depicted in Fig. 2. We refer to our supplementary video for live demos.

### 4.2 Baselines and Metrics

In our experiments, we evaluate the generated mesh quality as well as its consistency with the input sketch. For mesh quality, we report the Chamfer Distance (CD) to the target mesh. A smaller CD indicates better geometric consistency with the target. Additionally, for perceptual mesh quality evaluation we employ shading-image-based Fréchet Inception distance (FID) following MeshGPT [Siddiqui et al. 2023] and SENS [Binninger et al. 2024]. We also evaluate sketch-based CLIP [Radford et al. 2021] similarity, following LAS [Zheng et al. 2023], to measure the similarity between the generated mesh and the sketch. We additionally introduce sketch-based LPIPS [Zhang et al. 2018] to evaluate sketch-to-mesh correspondence: while CLIP shows the similarity of the global context, LPIPS focuses more on local features. For our method, we analyze runtime with the token generation speed in *tokens/second* (T/s).

We further conduct both unary and binary perceptual studies. In the unary study, participants evaluate mesh quality (GQ) and sketch matching (GM) for mesh generation. For mesh editing, they rate edited mesh quality (EQ), edited sketch matching (EM), and edited mesh consistency (EC) of the unedited part. Each is rated on a scale of 1 to 5 (=best). In the binary study, we ask participants to compare our method with baselines and select their preferred method. We report the percentages of preferences for our method compared to the baselines.

We compare with two state-of-the-art sketch-conditioned 3D generation methods, LAS [Zheng et al. 2023] and SENS [Binninger et al. 2024] as baselines. Since these methods produce signed distance fields or occupancy grids, we use marching cubes to convert their results to meshes. We alternatively use MeshAnythingV2 [Chen et al. 2024e] to post-process LAS and SENS results (LAS-MA and SENS-MA, respectively), producing more artistically-styled meshes for these baselines.

### 4.3 Experimental Setup

We use the test set described in Sec. 4.1 and automatically generate sketches from one of five views: top-left, top-front-left, top-front, top-front-right, or top-right, for the generation task. To further

Table 1. Evaluation on sketch-conditioned mesh generation. We compare with LAS [Zheng et al. 2023], SENS [Binninger et al. 2024], and further use MeshAnythingV2 (MA) [Chen et al. 2024e] to post-process LAS and SENS outputs. The unit of CD is 0.001. MeshPad outperforms baselines in both mesh quality and consistency with input sketches.

Dataset	Method	CD↓	LPIPS↓	CLIP↑	FID↓
ShapeNet	LAS	22.46	0.3309	93.01	47.07
	LAS-MA	29.69	0.3595	92.12	20.85
	SENS	8.95	0.2753	93.36	81.88
	SENS-MA	29.43	0.3348	91.88	42.93
	Ours	<b>6.20</b>	<b>0.1790</b>	<b>95.85</b>	<b>9.38</b>
IKEA	LAS	20.69	0.3281	93.70	68.51
	LAS-MA	26.54	0.3576	93.53	50.75
	SENS	8.76	0.2722	94.38	115.33
	SENS-MA	19.18	0.3037	94.37	99.08
	Ours	<b>6.78</b>	<b>0.1837</b>	<b>96.67</b>	<b>29.67</b>

show the robustness of our method, we use the IKEA dataset [Lim et al. 2013; Sun et al. 2018], which contains 188 furniture models. Additionally, we randomly select 50 shapes of airplanes, chairs, and lamps (on which SENS is trained) from the two datasets and manually edit the automatically generated sketches to build an evaluation dataset for sketch-based mesh editing.

As SENS is category-specific and is only trained on airplanes, chairs, and lamps, we evaluate it only on these categories. For the editing task, we let LAS generate from scratch conditioned on the edited sketch since it does not support localized editing; as SENS was designed for editing, and we ran its editing using its original design. For our method, while providing only the original sketch and the edited sketch, we first automatically generate input for deletion by identifying the difference between the two sketches, then perform the deletion-addition operation.

#### 4.4 Comparison to State of the Art

**Mesh Generation.** Tab. 1 evaluates MeshPad in comparison with state of the art on mesh generation. Quantitatively, our method outperforms baselines in all evaluation metrics, indicating superior mesh quality and sketch-to-mesh correspondence. We also conduct a perceptual study with 35 participants, and show results in Tabs. 2 and 3, further demonstrating user preference for our generated meshes. Fig. 7 provides qualitative comparison across the methods. While MeshAnythingV2 can convert marching cube meshes to meshes with more artist-reminiscent design, it is not robust enough to handle various artifacts in outputs of LAS and SENS (e.g., floaters or incomplete parts), resulting in an overall worse quality than our method, which bridges directly sketch to mesh.

**Mesh Editing.** Based on the results of the perceptual study, together with the sketch metrics reported in Tabs. 2 and 3, our method achieves the best LPIPS and CLIP scores among baselines and reaches the highest rating and preference among users. From the visual comparisons provided in Fig. 7, we notice that baseline methods suffer not only from poor editing results but also from inconsistency in unedited regions. This is because these methods regenerate the whole shape after the edit, can change regions not intended to be

Table 2. Sketch-based metrics and unary perceptual study ratings (ranged 1-5) on generation and editing results of our hand-drawn sketch evaluation set. We benchmark against LAS [Zheng et al. 2023] and SENS [Binninger et al. 2024], with outputs further refined using MeshAnythingV2 (MA) [Chen et al. 2024e]. For mesh generation, participants evaluate mesh quality (GQ) and sketch matching (GM). For mesh editing, participants rate edited mesh quality (EQ), edited sketch matching (EM), and edited mesh consistency (EC) of the unedited part.

Method	Sketch Matching		Gen. Rating		Edit Rating		
	LPIPS↓	CLIP↑	GQ↑	GM↑	EQ↑	EM↑	EC↑
LAS	0.3449	92.14	3.2	3.0	2.7	2.2	2.5
LAS-MA	0.3789	91.99	2.8	2.6	2.4	2.0	2.0
SENS	0.3179	91.49	3.4	3.5	2.9	1.8	3.7
SENS-MA	0.3651	90.20	2.7	2.8	2.1	1.6	2.5
Ours	<b>0.2218</b>	<b>95.71</b>	<b>4.3</b>	<b>4.3</b>	<b>4.3</b>	<b>4.2</b>	<b>4.3</b>

Table 3. Binary perceptual study. Participants choose their preferred output between our method and each baseline (LAS [Zheng et al. 2023], SENS [Binninger et al. 2024], and their results post-processed by MeshAnythingV2 (MA) [Chen et al. 2024e]). Our method is preferred by a large margin for both generation and editing.

Operation	LAS	LAS-MA	SENS	SENS-MA
Generation	93.3%	94.2%	83.7%	91.0%
Editing	94.4%	96.5%	91.9%	94.4%

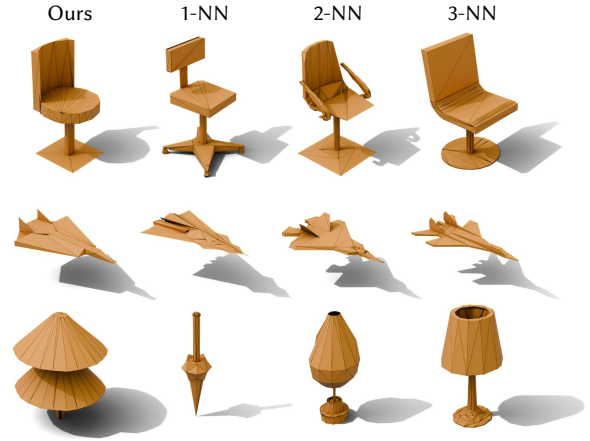


Fig. 5. Novelty of generated shapes. We retrieve the nearest neighbors of the generated meshes by first aligning them to each train mesh with Iterative Closest Point (ICP) and then computing the Chamfer distance. Our method can generate new shapes different from those in the train set.

edited. Our method solves this problem by decoupling the editing procedure into deletion and addition, ensuring that only edited regions are changed.

**Novelty Analysis.** Fig. 5 shows a qualitative novelty analysis, retrieving for our generated meshes the 3 nearest neighbors from the training set, based on Chamfer distance. Our generated shapes differ from their nearest neighbors in both overall shape and triangulation, which demonstrates that our method can generate new shapes.

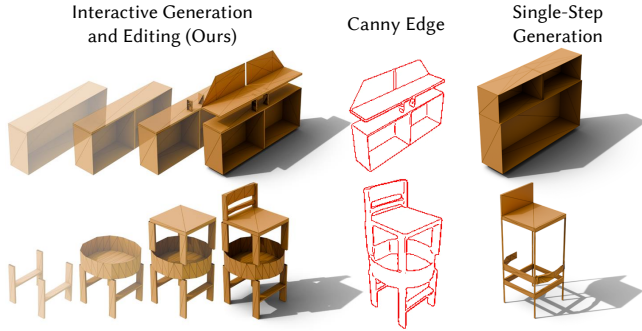


Fig. 6. Comparisons between our interactive generation and editing vs. single-step generation. **Left:** meshes interactively created using our method, which effectively uses multiple localized generation steps to achieve high complexity. **Middle:** synthetic sketches generated from the final meshes via Canny Edge detection. **Right:** meshes generated by applying one pass of the addition network (without iterative editing) on the middle sketches. Our interactive editing pipeline enables creating intricate shapes that can be challenging to generate in one step.

**Generating Complex Shapes through Interactive Editing.** Our interactive mesh editing enables not only an iterative creation process, but its localized editing focus enables construction of complex 3D shapes by decomposing their generation into a sequence of simpler part generations. As a result, artists can use our method to create a larger variety of complex shapes than the single-step generation, as demonstrated in Fig. 6. We refer to our supplementary video for more interactive modelings in action.

#### 4.5 Ablations

Tab. 4 ablates our vertex-aligned speculator design choices. We conduct ablation studies on three variants of the addition network: without speculator, without vertex-aligned decoding (with the same decoding length of 2), and without joint training with the OPT.

**Joint training provides context-rich hidden states as speculator input.** We find that the vanilla speculator training scheme with frozen transformer [Wertheimer et al. 2024] does not work in our mesh generation setting, as the hidden states from our pre-trained transformer do not contain enough contextual information. As shown in Tab. 4, by instead training the speculator jointly with the OPT, our model achieves strong mesh quality performance. In contrast, training the speculator with the OPT frozen results in poor performance. This indicates the OPT learns to encode contexts into the hidden states when jointly trained.

**Vertex-alignment preserves mesh quality while achieving comparable speedup as vanilla MLP speculator.** Comparing no speculator (w/o speculator) and speculator without vertex alignment (w/o vert-alignment), we can see that the speculator, without aligning to vertex tokens, results in a notable speedup, but at large penalty cost in mesh quality and sketch-to-mesh correspondence. By aligning the speculator to vertex tokens, our method reaches the same level of sketch-to-mesh correspondence as the no speculator version while maintaining the naive speculator’s advantage in

Table 4. Ablation study. We ablate our speculator, vertex alignment of our speculator (using a common MLP speculator [Wertheimer et al. 2024] with the same length of 2), and its joint training with our mesh transformer. The unit of CD is 0.001. T/s represents tokens per second and is measured on NVIDIA A100. Our vertex-aligned speculator accelerates generation by 2.16× without loss in mesh quality. Compared to an MLP speculator without vertex-alignment, which suffers from quality loss, our method runs at a comparable speed.

Method	Quality Metrics				Speed T/s↑
	CD↓	LPIPS↓	CLIP↑	FID↓	
w/o speculator	7.66	<b>0.1765</b>	95.59	32.59	60.7
w/o vert-alignment	9.00	0.1992	94.43	35.65	<b>138.9</b>
w/o joint training	57.13	0.5134	84.52	211.46	125.3
Ours	<b>6.78</b>	<u>0.1837</u>	<b>96.67</b>	<b>29.67</b>	<u>131.1</u>

generation speed. Additionally, applying the vertex-aligned speculator results in slightly higher metrics in mesh quality. This is likely due to the vertex-aligned speculator reducing the complexity of the linear prediction head. Rather than predicting control tokens and all  $x$ ,  $y$ , and  $z$  coordinate tokens, it is trained to predict only control tokens and  $x$  coordinate tokens, which reduces the overall prediction error. Thus, equipped with the vertex-aligned speculator, our method achieves strong performance and fast generation speeds (approximately 26.7 faces per second considering the average face density of the mesh sequences).

**Runtime.** Our mesh addition, which typically generates  $\approx 1/5$  of a shape, runs in about 1 to 5 seconds (depending on the number of faces added), enabling interactive runtimes for editing.

**Limitations.** While our method produces interactive editing for 3D meshes, our transformer-based approach is bound by the memory size to a maximum sequence length, resulting in a limited number of mesh triangles (768 triangles in our experiments) that can be processed. Although there are methods [Hao et al. 2024; Tang et al. 2024] that extend the limit of the token amount in mesh generation, the upper bound (thousands of triangles) is still far below the requirement of modern computer graphics applications (millions of triangles). Thus, we demonstrate the efficacy of our approach on isolated 3D shapes, but would require paradigms in learned mesh representations in order to generate and edit larger-scale scenes.

## 5 CONCLUSION

MeshPad introduces interactive editing into autoregressive mesh generation, by decomposing editing into addition and deletion operations on sequentialized mesh tokens. In contrast to existing works which focus on full shape generation, MeshPad enables fine-grained and localized control over the artistic generation process. To enable interactive feedback, our vertex-aligned speculator notably speeds up mesh face generation, running in just a few seconds in response to user sketch updates. Our sketch-conditioned approach also enables ease of use in creation of complex 3D meshes from novice users. We believe that interactive mesh editing represents a significant step toward democratizing content creation, enabling everyone to create artist-reminiscent 3D meshes.

## ACKNOWLEDGMENTS

This work was funded by AUDI AG. Lei Li and Angela Dai were supported by the ERC Starting Grant SpatialSem (101076253) and Matthias Nießner by the ERC Consolidator Grant Gen3D (101171131).

## REFERENCES

- Abubakar Abid, Ali Abdalla, Ali Abid, Dawood Khan, Abdulrahman Alfozan, and James Zou. 2019. Gradio: Hassle-Free Sharing and Testing of ML Models in the Wild. *arXiv preprint arXiv:1906.02569* (2019).
- Noam Aigerman, Kunal Gupta, Vladimir G. Kim, Siddhartha Chaudhuri, Jun Saito, and Thibault Groueix. 2022. Neural jacobian fields: learning intrinsic mappings of arbitrary meshes. 41, 4, Article 109 (2022), 17 pages. doi:10.1145/3528223.3530141
- Antonio Alliegro, Yawar Siddiqui, Tatiana Tommasi, and Matthias Nießner. 2023. PolyDiff: Generating 3D Polygonal Meshes with Diffusion Models. *arXiv:2312.11417 [cs.CV]* <https://arxiv.org/abs/2312.11417>
- Maciej Bala, Yin Cui, Yifan Ding, Yunhao Ge, Zekun Hao, Jon Hasselgren, Jacob Huffman, Jingyi Jin, JP Lewis, Zhaoshuo Li, et al. 2024. Edify 3D: Scalable High-Quality 3D Asset Generation. *arXiv preprint arXiv:2411.07135* (2024).
- Hmrishav Bandyopadhyay, Subhadeep Koley, Ayan Das, Ayan Kumar Bhunia, Aneeshan Sain, Pinaki Nath Chowdhury, Tao Xiang, and Yi-Zhe Song. 2024. Doodle Your 3D: From Abstract Freehand Sketches to Precise 3D Shapes. *CVPR* (2024).
- Amir Barda, Matheus Gadelha, Vladimir G Kim, Noam Aigerman, Amit H Bermano, and Thibault Groueix. 2024. Instant3dit: Multiview Inpainting for Fast Editing of 3D Objects. *arXiv preprint arXiv:2412.00518* (2024).
- Alexandre Binninger, Amir Hertz, Olga Sorkine-Hornung, Daniel Cohen-Or, and Raja Giryes. 2024. SENS: Part-Aware Sketch-based Implicit Neural Shape Modeling. *Computer Graphics Forum (Proceedings of EUROGRAPHICS 2024)* 43, 2 (2024).
- Ricardo Cabello and Contributors. 2010. Three.js: JavaScript 3D library. <https://threejs.org/>. Accessed: 2025-01-22.
- Angel X Chang, Thomas Funkhouser, Leonidas Guibas, Pat Hanrahan, Qixing Huang, Zimo Li, Silvio Savarese, Manolis Savva, Shuran Song, Hao Su, et al. 2015. Shapenet: An information-rich 3d model repository. *arXiv preprint arXiv:1512.03012* (2015).
- Charlie Chen, Sebastian Borgeaud, Geoffrey Irving, Jean-Baptiste Lespiau, Laurent Sifre, and John Jumper. 2023a. Accelerating large language model decoding with speculative sampling. *arXiv preprint arXiv:2302.01318* (2023).
- Hansheng Chen, Ruoxi Shi, Yulin Liu, Bokui Shen, Jiayuan Gu, Gordon Wetzstein, Hao Su, and Leonidas Guibas. 2024d. Generic 3D Diffusion Adapter Using Controlled Multi-View Editing. *arXiv preprint arXiv:2403.12032* (2024).
- Minghao Chen, Roman Shapovalov, Iro Laina, Tom Monnier, Jianyuan Wang, David Novotny, and Andrea Vedaldi. 2024c. PartGen: Part-level 3D Generation and Reconstruction with Multi-View Diffusion Models. *arXiv preprint arXiv:2412.18608* (2024).
- Rui Chen, Yongwei Chen, Ningxin Jiao, and Kui Jia. 2023b. Fantasia3D: Disentangling Geometry and Appearance for High-quality Text-to-3D Content Creation. In *Proceedings of the IEEE/CVF International Conference on Computer Vision (ICCV)*. 22246–22256.
- Yiwen Chen, Zilong Chen, Chi Zhang, Feng Wang, Xiaofeng Yang, Yikai Wang, Zhonggang Cai, Lei Yang, Huaping Liu, and Guosheng Lin. 2024a. GaussianEditor: Swift and Controllable 3D Editing with Gaussian Splatting. In *Proceedings of the IEEE/CVF Conference on Computer Vision and Pattern Recognition (CVPR)*. 21476–21485.
- Yiwen Chen, Tong He, Di Huang, Weicai Ye, Sijin Chen, Jiayang Tang, Xin Chen, Zhonggang Cai, Lei Yang, Gang Yu, Guosheng Lin, and Chi Zhang. 2024b. MeshAnything: Artist-Created Mesh Generation with Autoregressive Transformers. *arXiv:2406.10163 [cs.CV]*
- Yiwen Chen, Yikai Wang, Yihao Luo, Zhengyi Wang, Zilong Chen, Jun Zhu, Chi Zhang, and Guosheng Lin. 2024e. MeshAnything V2: Artist-Created Mesh Generation With Adjacent Mesh Tokenization. *arXiv:2408.02555 [cs.CV]* <https://arxiv.org/abs/2408.02555>
- Angela Dai, Christian Diller, and Matthias Nießner. 2020. Sg-nn: Sparse generative neural networks for self-supervised scene completion of rgb-d scans. In *Proceedings of the IEEE/CVF Conference on Computer Vision and Pattern Recognition*. 849–858.
- Angela Dai and Matthias Nießner. 2019. Scan2mesh: From unstructured range scans to 3d meshes. In *Proceedings of the IEEE/CVF Conference on Computer Vision and Pattern Recognition*. 5574–5583.
- Angela Dai, Charles Ruizhongtai Qi, and Matthias Nießner. 2017. Shape completion using 3d-encoder-predictor cnns and shape synthesis. In *Proceedings of the IEEE conference on computer vision and pattern recognition*. 5868–5877.
- Mathias Eitz, Ronald Richter, Tamy Boubekeur, Kristian Hildebrand, and Marc Alexa. 2012. Sketch-based shape retrieval. 31, 4, Article 31 (July 2012), 10 pages. doi:10.1145/2185520.2185527
- Mohamed Elrefaie, Faez Ahmed, and Angela Dai. 2024. Drivaernet: A parametric car dataset for data-driven aerodynamic design and graph-based drag prediction. In *International Design Engineering Technical Conferences and Computers and Information in Engineering Conference*, Vol. 88360. American Society of Mechanical Engineers, V03AT03A019.
- Thomas Funkhouser, Patrick Min, Michael Kazhdan, Joyce Chen, Alex Halderman, David Dobkin, and David Jacobs. 2003. A search engine for 3D models. *ACM Trans. Graph.* 22, 1 (Jan. 2003), 83–105. doi:10.1145/588272.588279
- William Gao, Noam Aigerman, Thibault Groueix, Vova Kim, and Rana Hanocka. 2023. Textdeformer: Geometry manipulation using text guidance. In *ACM SIGGRAPH 2023 Conference Proceedings*. 1–11.
- Will Gao, Dilin Wang, Yuchen Fan, Aljaz Bozic, Tuur Stuyck, Zhengqin Li, Zhao Dong, Rakesh Ranjan, and Nikolaos Sarafianos. 2024. 3D Mesh Editing using Masked LRMs. *arXiv preprint arXiv:2412.08641* (2024).
- Thibault Groueix, Matthew Fisher, Vladimir G Kim, Bryan C Russell, and Mathieu Aubry. 2018. A papier-mâché approach to learning 3d surface generation. In *Proceedings of the IEEE conference on computer vision and pattern recognition*. 216–224.
- Zekun Hao, David W Romero, Tsung-Yi Lin, and Ming-Yu Liu. 2024. Meshtron: High-Fidelity, Artist-Like 3D Mesh Generation at Scale. *arXiv preprint arXiv:2412.09548* (2024).
- Amir Hertz, Or Perel, Raja Giryes, Olga Sorkine-Hornung, and Daniel Cohen-Or. 2022. Spaghetti: Editing implicit shapes through part aware generation. *ACM Transactions on Graphics (TOG)* 41, 4 (2022), 1–20.
- Takeo Igarashi, Satoshi Matsuoka, and Hidehiko Tanaka. 1999. Teddy: a sketching interface for 3D freeform design. In *Proceedings of the 26th Annual Conference on Computer Graphics and Interactive Techniques (SIGGRAPH '99)*. ACM Press/Addison-Wesley Publishing Co., USA, 409–416. doi:10.1145/311535.311602
- Bernhard Kerbl, Georgios Kopanas, Thomas Leimkühler, and George Drettakis. 2023. 3D Gaussian splatting for real-time radiance field rendering. *ACM Trans. Graph.* 42, 4 (2023), 139–1.
- Umar Khalid, Hasan Iqbal, Nazmul Karim, Muhammad Tayyab, Jing Hua, and Chen Chen. 2025. LatentEditor: Text Driven Local Editing of 3D Scenes. In *Computer Vision – ECCV 2024*. Aleš Leonardis, Elisa Ricci, Stefan Roth, Olga Russakovsky, Torsten Sattler, and Gül Varol (Eds.). Springer Nature Switzerland, Cham, 364–380.
- Jul Koo, Seungwoo Yoo, Minh Hieu Nguyen, and Minhuk Sung. 2023. Salad: Part-level latent diffusion for 3d shape generation and manipulation. In *Proceedings of the IEEE/CVF International Conference on Computer Vision*. 14441–14451.
- Yaniv Leviathan, Matan Kalman, and Yossi Matias. 2023. Fast Inference from Transformers via Speculative Decoding. In *Proceedings of the 40th International Conference on Machine Learning (Proceedings of Machine Learning Research, Vol. 202)*. Andreas Krause, Emma Brunskill, Kyunghyun Cho, Barbara Engelhardt, Sivan Sabato, and Jonathan Scarlett (Eds.). PMLR, 19274–19286.
- Joseph J Lim, Hamed Pirsiavash, and Antonio Torralba. 2013. Parsing ikea objects: Fine pose estimation. In *Proceedings of the IEEE international conference on computer vision*. 2992–2999.
- Chen-Hsuan Lin, Jun Gao, Luming Tang, Towaki Takikawa, Xiao-hui Zeng, Xun Huang, Karsten Kreis, Sanja Fidler, Ming-Yu Liu, and Tsung-Yi Lin. 2023. Magic3D: High-Resolution Text-to-3D Content Creation. In *Proceedings of the IEEE/CVF Conference on Computer Vision and Pattern Recognition (CVPR)*. 300–309.
- Feng-Lin Liu, Hongbo Fu, Yu-Kun Lai, and Lin Gao. 2024. Sketchdream: Sketch-based text-to-3d generation and editing. *ACM Transactions on Graphics (TOG)* 43, 4 (2024), 1–13.
- Xinyao Liu, Kai Xu, Yuhang Huang, Renjiao Yi, and Chenyang Zhu. 2025. MaskEditor: Instruct 3D Object Editing with Learned Masks. In *Pattern Recognition and Computer Vision*, Zhouchen Lin, Ming-Ming Cheng, Ran He, Kurban Ubul, Wushouer Silamu, Hongbin Zha, Jie Zhou, and Cheng-Lin Liu (Eds.). Springer Nature Singapore, Singapore, 285–298.
- Xupeng Miao, Gabriele Oliaro, Zhihao Zhang, Xinhao Cheng, Zeyu Wang, Zhengxin Zhang, Rae Ying Yee Wong, Alan Zhu, Lijie Yang, Xiaoxiang Shi, et al. 2023. SpecInfer: Accelerating Generative Large Language Model Serving with Tree-based Speculative Inference and Verification. *arXiv preprint arXiv:2305.09781* (2023).
- Aryan Mikaeili, Or Perel, Mehdi Safaei, Daniel Cohen-Or, and Ali Mahdavi-Amiri. 2023. Sked: Sketch-guided text-based 3d editing. In *Proceedings of the IEEE/CVF International Conference on Computer Vision*. 14607–14619.
- Ben Mildenhall, Pratul P Srinivasan, Matthew Tancik, Jonathan T Barron, Ravi Ramamoorthi, and Ren Ng. 2021. Nerf: Representing scenes as neural radiance fields for view synthesis. *Commun. ACM* 65, 1 (2021), 99–106.
- Charlie Nash, Yaroslav Ganin, S. M. Ali Eslami, and Peter W. Battaglia. 2020. PolyGen: an autoregressive generative model of 3D meshes. In *Proceedings of the 37th International Conference on Machine Learning (ICML '20)*. JMLR.org, Article 669, 10 pages.
- Andrew Nealen, Takeo Igarashi, Olga Sorkine, and Marc Alexa. 2007. FiberMesh: designing freeform surfaces with 3D curves. *ACM Trans. Graph.* 26, 3 (July 2007), 41–es. doi:10.1145/1276377.1276429
- Ben Poole, Ajay Jain, Jonathan T. Barron, and Ben Mildenhall. 2023. DreamFusion: Text-to-3D using 2D Diffusion. In *The Eleventh International Conference on Learning*



- Representations*. <https://openreview.net/forum?id=FjNys5c7VyY>
- Xuelin Qian, Yu Wang, Simian Luo, Yinda Zhang, Ying Tai, Zhenyu Zhang, Chengjie Wang, Xiangyang Xue, Bo Zhao, Tiejun Huang, Yunsheng Wu, and Yanwei Fu. 2024. Pushing Auto-regressive Models for 3D Shape Generation at Capacity and Scalability. *arXiv:2402.12225* [cs.CV]
- Alec Radford, Jong Wook Kim, Chris Hallacy, Aditya Ramesh, Gabriel Goh, Sandhini Agarwal, Girish Sastry, Amanda Askell, Pamela Mishkin, Jack Clark, et al. 2021. Learning transferable visual models from natural language supervision. In *International conference on machine learning*. PMLR, 8748–8763.
- Mike Ranzinger, Greg Heinrich, Jan Kautz, and Pavlo Molchanov. 2024. AM-RADIO: Agglomerative Vision Foundation Model Reduce All Domains Into One. In *Proceedings of the IEEE/CVF Conference on Computer Vision and Pattern Recognition (CVPR)*. 12490–12500.
- Xuanchi Ren, Jiahui Huang, Xiaohui Zeng, Ken Museth, Sanja Fidler, and Francis Williams. 2024. Xcube: Large-scale 3d generative modeling using sparse voxel hierarchies. In *Proceedings of the IEEE/CVF Conference on Computer Vision and Pattern Recognition*. 4209–4219.
- Daniel Korth Robin Borth. 2024. Sketch2Shape: Single-View Sketch-Based 3D Reconstruction via Multi-View Differentiable Rendering. (2024).
- Yawar Siddiqui, Antonio Alliegro, Alexey Artemov, Tatiana Tommasi, Daniele Sirigatti, Vladislav Rosov, Angela Dai, and Matthias Nießner. 2023. MeshGPT: Generating Triangle Meshes with Decoder-Only Transformers. *arXiv preprint arXiv:2311.15475* (2023).
- Yawar Siddiqui, Tom Monnier, Filippos Kokkinos, Mahendra Kariya, Yanir Kleiman, Emilien Garreau, Oran Gafni, Natalia Neverova, Andrea Vedaldi, Roman Shapovalov, and David Novotny. 2024. Meta 3D AssetGen: Text-to-Mesh Generation with High-Quality Geometry, Texture, and PBR Materials. *arXiv* (2024).
- Xingyuan Sun, Jiajun Wu, Xiuming Zhang, Zhoutong Zhang, Chengkai Zhang, Tianfan Xue, Joshua B Tenenbaum, and William T Freeman. 2018. Pix3d: Dataset and methods for single-image 3d shape modeling. In *Proceedings of the IEEE conference on computer vision and pattern recognition*. 2974–2983.
- Jiaxiang Tang, Zhaoshuo Li, Zekun Hao, Xian Liu, Gang Zeng, Ming-Yu Liu, and Qinsheng Zhang. 2024. EdgeRunner: Auto-regressive Auto-encoder for Artistic Mesh Generation. *arXiv preprint arXiv:2409.18114* (2024).
- Jiapeng Tang, Lev Markhasin, Bi Wang, Justus Thies, and Matthias Nießner. 2022. Neural shape deformation priors. *Advances in Neural Information Processing Systems* 35 (2022), 17117–17132.
- Arash Vahdat, Francis Williams, Zan Gojcic, Or Litany, Sanja Fidler, Karsten Kreis, et al. 2022. Lion: Latent point diffusion models for 3d shape generation. *Advances in Neural Information Processing Systems* 35 (2022), 10021–10039.
- Davis Wertheimer, Joshua Rosenkranz, Thomas Parnell, Sahil Suneja, Pavithra Rangathan, Raghu Ganti, and Mudhakar Srivatsa. 2024. Accelerating Production LLMs with Combined Token/Embedding Speculators. *arXiv preprint arXiv:2404.19124* (2024).
- Jiale Xu, Xintao Wang, Yan-Pei Cao, Weihao Cheng, Ying Shan, and Shenghua Gao. 2023. InstructP2P: Learning to Edit 3D Point Clouds with Text Instructions. *arXiv:2306.07154* [cs.CV] <https://arxiv.org/abs/2306.07154>
- Guandao Yang, Xun Huang, Zekun Hao, Ming-Yu Liu, Serge Belongie, and Bharath Hariharan. 2019. Pointflow: 3d point cloud generation with continuous normalizing flows. In *Proceedings of the IEEE/CVF international conference on computer vision*. 4541–4550.
- Richard Zhang, Phillip Isola, Alexei A Efros, Eli Shechtman, and Oliver Wang. 2018. The unreasonable effectiveness of deep features as a perceptual metric. In *Proceedings of the IEEE conference on computer vision and pattern recognition*. 586–595.
- Susan Zhang, Stephen Roller, Naman Goyal, Mikel Artetxe, Moya Chen, Shuohui Chen, Christopher Dewan, Mona Diab, Xian Li, Xi Victoria Lin, et al. 2022. Opt: Open pre-trained transformer language models. *arXiv preprint arXiv:2205.01068* (2022).
- Wang Zhao, Yan-Pei Cao, Jiale Xu, Yuejiang Dong, and Ying Shan. 2024. DI-PCG: Diffusion-based Efficient Inverse Procedural Content Generation for High-quality 3D Asset Creation. *arXiv preprint arXiv:2412.15200* (2024).
- Xin-Yang Zheng, Hao Pan, Peng-Shuai Wang, Xin Tong, Yang Liu, and Heung-Yeung Shum. 2023. Locally Attentional SDF Diffusion for Controllable 3D Shape Generation. *ACM Transactions on Graphics (SIGGRAPH)* 42, 4 (2023).
- Linqi Zhou, Yilun Du, and Jiajun Wu. 2021. 3d shape generation and completion through point-voxel diffusion. In *Proceedings of the IEEE/CVF international conference on computer vision*. 5826–5835.

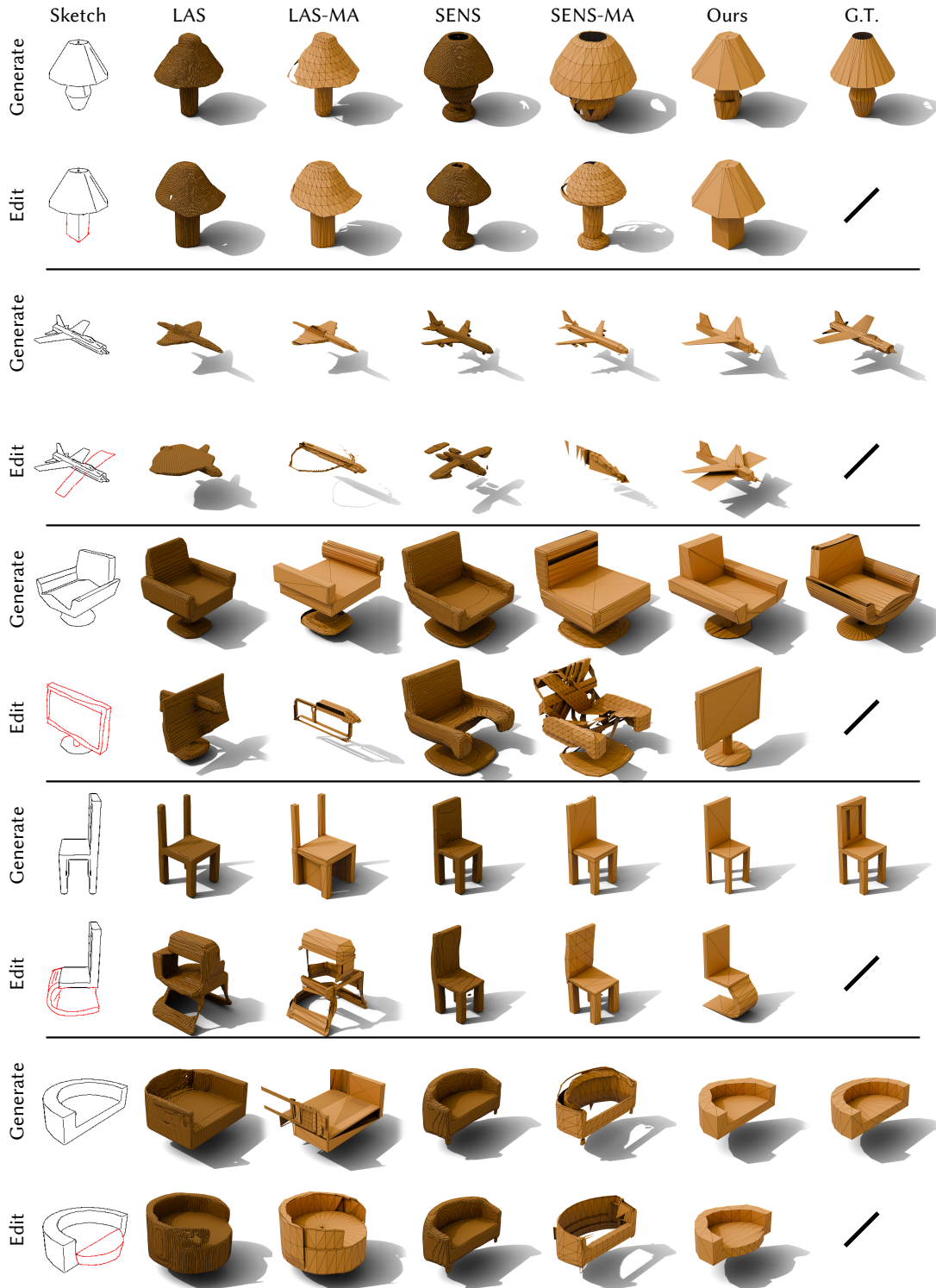


Fig. 7. Visual comparison of generation and editing results. We show generation and editing results of LAS [Zheng et al. 2023], SENS [Binninger et al. 2024], and their results post-processed by MeshAnythingV2 (MA) [Chen et al. 2024e]. Our method produces 3D meshes that not only match the sketch inputs and edits, but also offer high fidelity.

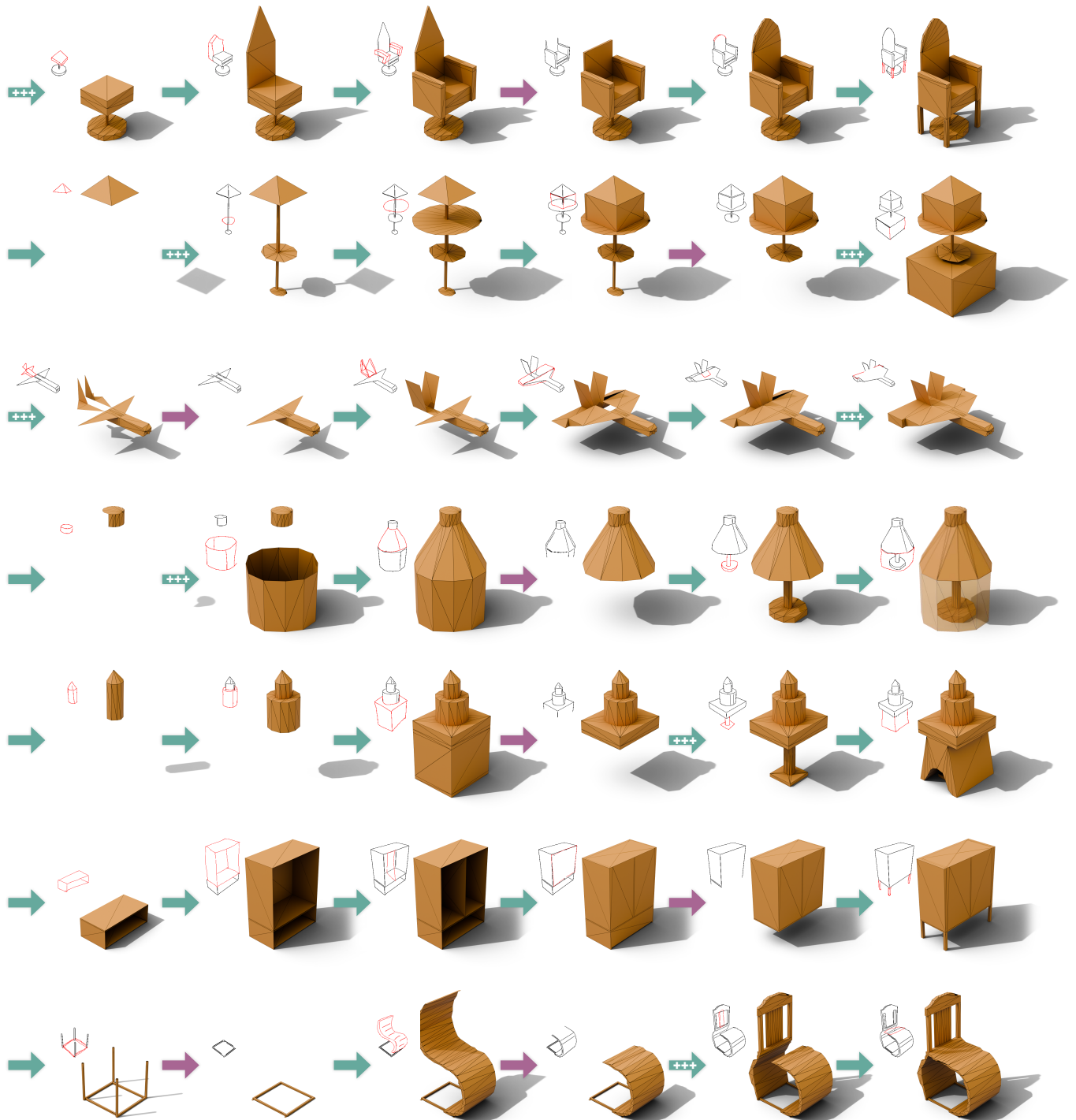


Fig. 8. Sequence visualization of mesh creation with MeshPad. We show the input sketch on the top left of each of our method outputs. Green and purple arrows represent addition and deletion, respectively. The “+++” inside a green arrow indicates multiple addition steps.

# Supplementary Material for MeshPad: Interactive Sketch Conditioned Artistic-designed Mesh Generation and Editing

In this material, we first introduce more details of our self-supervised data processing in Sec. 6. Then, showcase two applications with our method - image-conditioned generation and direct mesh editing in Sec. 7 and Sec. 8, respectively. Next, we provide more visual evaluation results in Sec. 9 followed by more details and results from our perceptual study in Sec. 10.

## 6 DATA GENERATION DETAILS

In this section, we provide additional details for our data generation process (Sec. 3.4).

**Random sampling of volumes.** To sample volumes that satisfy  $\mathcal{L}_k \subseteq \mathcal{L}$ , we first randomly define two volumes  $\mathcal{L}_{\{a,b\}}$  within the bounding volume (assuming a unit cube) of the complete mesh  $\mathcal{M}_c$ . For each volume  $\tilde{\mathcal{L}}$  of  $\mathcal{L}_{\{a,b\}}$ , we sample the volume as following: first, randomly choose an axis  $i$  from  $\{1, 2, 3\}$  indicating the  $x$ ,  $y$ , or  $z$  axis, then randomly select one region  $\mathcal{R}$  from the four candidates:  $[-\infty, a]$ ,  $[a, +\infty]$ ,  $[b - c, b + c]$ ,  $[-\infty, b - c] \cup [b + c, +\infty]$ , where  $a \in [0.2, 0.8]$ ,  $b \in [0.4, 0.6]$  and  $c \in [0.1, 0.4]$  are uniformly sampled within their defined range. The sampled volume is then defined as:

$$\tilde{\mathcal{L}} = \{p \in \mathbb{R}^3 | p_i \in \mathcal{R}\}. \quad (7)$$

Then we define:

$$\mathcal{L}_k = \mathcal{L}_a; \quad \mathcal{L} = \mathcal{L}_a \cup \mathcal{L}_b, \quad (8)$$

which ensures that  $\mathcal{L}_k \subseteq \mathcal{L}$ .

After sampling both volumes, it can happen that  $\mathcal{L}_b \subseteq \mathcal{L}_a$ , and as a result,  $\mathcal{L} = \mathcal{L}_k$  and thus the editing part  $\mathcal{M}_r$  is empty. To avoid this, we manually set  $\mathcal{L}_b = \mathbb{R}^3$  in this case so that it contains the entire mesh (that is, a mesh completion task for addition).

The random volume sampling, while effective, can produce data samples that are not well-suited for training. For instance, the target mesh  $\mathcal{M}$  for addition could be close to the complete mesh  $\mathcal{M}_c$  with just a few triangles missing, and that the sketch is also close to the full sketch of  $\mathcal{M}_c$ . As a consequence, the model would learn to generate a mesh with missing triangles, even when the user provides a complete sketch. To address this issue, we additionally check the coverage of the visibility mask of  $\mathcal{M}$  to the complete mesh's ( $\mathcal{M}_c$ ) and set  $\mathcal{L}_b = \mathbb{R}^3$  if the coverage is greater than 95%.

**Sketch generation.** We mentioned in Sec. 3.4 to use a visibility mask of  $\mathcal{M}_r$  for splitting line strokes in  $\mathcal{I}$ . In practice, the line strokes from the Canny edge detector could lie outside the mask by 1 pixel. Therefore, we dilate the visibility mask by 1 pixel before collecting  $\mathcal{I}_r$ .

**Mesh and sketch augmentations.** During training, we apply random axis independent scaling to the mesh, with a scaling factor uniformly sampled in  $[0.9, 1.1]$  on each axis. For the sketch, we apply a random affine transformation and a random elastic transformation to fill the domain gap between generated sketches and human drawings.

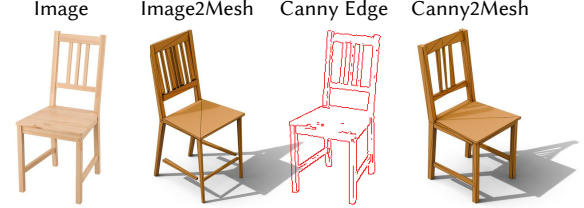


Fig. 9. Image to mesh results. Benefiting from the large image foundation model RADIO, our method generalizes to image-conditioning without additional training. For better image matching and mesh quality, users can pre-process the image to get a canny edge for conditioning.

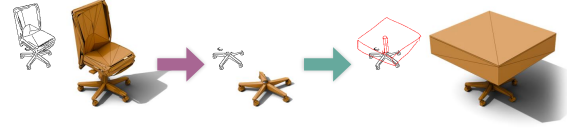


Fig. 10. Our method allows us to edit directly on a given mesh (created manually or with other methods). We first load a mesh of an office chair, and automatically generate the corresponding rendered sketch. We can then delete the upper part and add a square tabletop to build a movable table.

## 7 IMAGE-CONDITIONED MESH GENERATION

While our method is not trained on images, it generalizes well to image-conditioning, taking advantage of the large image foundation model RADIO [Ranzinger et al. 2024]. It requires no re-training nor any adaptations to the pipeline to use our model for image-conditioned mesh generation. In Fig. 9, we show an example of image-conditioned generation with our method. It is worth mentioning that the mesh quality and image-to-mesh correspondence are lower for image-conditioned generation compared to sketch-conditioned generation. A simple pre-processing to get the canny edge for conditioning would boost the performance of our method.

## 8 DIRECT MESH EDITING

Another benefit of using mesh as an underlying representation is that we could edit directly on a given mesh. Other methods, such as SENS [Binninger et al. 2024], that perform editing on latent spaces struggle at editing a given mesh as it is tricky to convert the mesh to the model input. The common way is to encode the mesh to the latent space and feed it to the model. Consequently, there is no guarantee that the unedited part will remain unchanged due to the error of encoding and decoding. Our method naturally addresses this issue using explicit mesh representation as model input. This allows us to edit a given mesh without worrying about changing the unedited parts. In Fig. 10, we show an example of editing a given



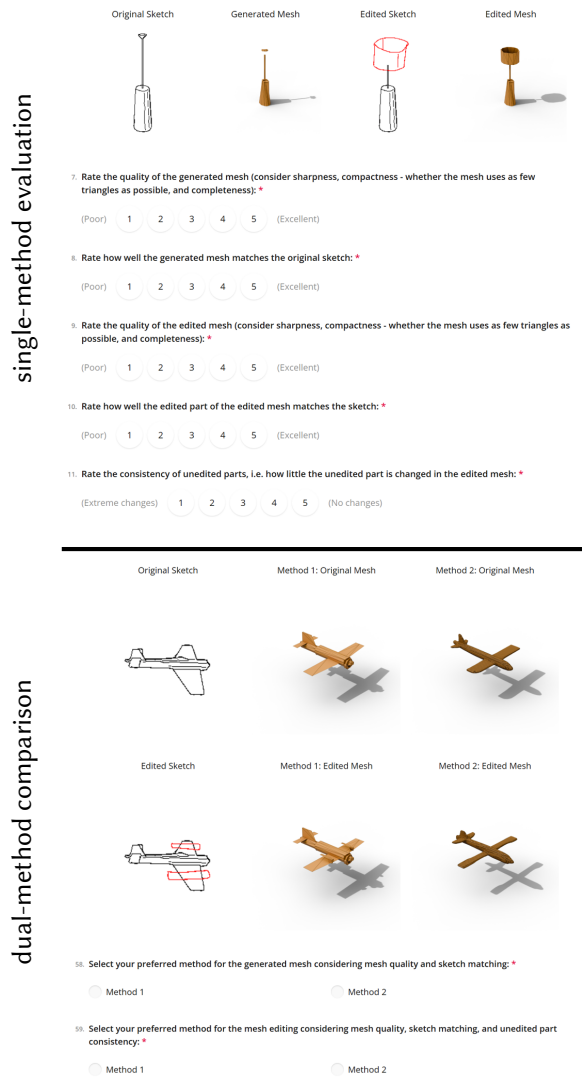


Fig. 12. Screenshot of our perceptual study. **Left:** single-method evaluation. **Right:** dual-method comparison. Each participant is required to complete 10 single-method evaluations and 10 dual-method comparison tasks.

Table 5. User ratings (ranged 1-5) on generation and editing results of our hand-drawn sketch evaluation set. We benchmark against LAS [Zheng et al. 2023] and SENS [Binniger et al. 2024], with outputs further refined using MeshAnythingV2 (MA) [Chen et al. 2024e] as a post-processing baseline. For mesh generation, participants evaluate mesh quality (GQ) and sketch matching (GM). For mesh editing, participants rate edited mesh quality (EQ), edited sketch matching (EM), and edited mesh consistency (EC) of the unedited part.

Method	Generation Rating		Editing Rating		
	GQ↑	GM↑	EQ↑	EM↑	EC↑
LAS	3.2(1.1)	3.0(1.2)	2.7(1.1)	2.2(1.1)	2.5(1.3)
LAS-MA	2.8(1.2)	2.6(1.2)	2.4(1.3)	2.0(1.1)	2.0(1.1)
SENS	3.4(1.2)	3.5(1.1)	2.9(1.2)	1.8(1.0)	3.7(1.6)
SENS-MA	2.7(1.4)	2.8(1.4)	2.1(1.4)	1.6(1.1)	2.5(1.3)
Ours	<b>4.3(0.9)</b>	<b>4.3(0.8)</b>	<b>4.3(0.8)</b>	<b>4.2(0.9)</b>	<b>4.3(1.0)</b>

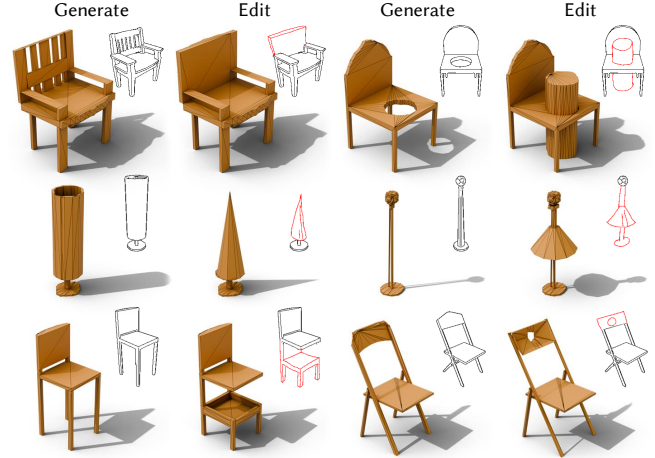


Fig. 11. Visual results of our method on our hand-drawn dataset. Our method successfully performs a variety of edits, from local changes to edits that affect the majority of the shape.

mesh. After loading the mesh and generating the sketch, we could perform addition and deletion as if the mesh is generated by the model.

## 9 ADDITIONAL VISUAL RESULTS

We provide more mesh generation and editing results of our method in Fig. 11, as a complement to Fig. 7. Note that our hand-drawn sketch editing dataset, while containing only 50 meshes, covers a large variety of editing tasks that are common in interactive mesh editing, from small local changes to global shape structure adjustments. Thus, it serves as a strong and challenging benchmark for sketch-based mesh editing. While trained only on self-supervised data (Sec. 3.4) without any data from real artist drawings, our method generalizes to these tasks proposed with human drawing, showing consistent performance across diverse editing tasks. This highlights the effectiveness of our self-supervised data processing approach.

## 10 PERCEPTUAL STUDY DETAILS

In our perceptual study, we ask each participant to do 10 single-method evaluation tasks and 10 dual-method comparison (ours vs. baseline) tasks. Fig. 12 shows the UI for our perceptual study. The samples used for the questions are randomly chosen from all mesh editing results of all methods and are different for each participant. Our participants have a large variety: from professional artists to hobbyists, students, and individuals with no prior artistic experience.

We show in Tab. 5 again the unary user rating with the standard deviation. With the smallest deviation observed in all subjects, we show a high agreement among participants regarding the performance of our method.